ASM | mBio

| Environmental Microbiology | Research Article

Light-directed biofilm formation reveals the functional contributions of periplasmic cytochromes to the electrochemical activity of *Shewanella oneidensis*

Fengjie Zhao,[1] Christina M. Niman,[1] Marko S. Chavez,[1,2] Joshua T. Atkinson,[1,2,3] Bridget E. Conley,[4] Jeffrey A. Gralnick,[4] James Q. Boedicker,[1,5] Mohamed Y. El-Naggar[1,5,6]

AUTHOR AFFILIATIONS See affiliation list on p. 13.

ABSTRACT *Shewanella oneidensis* MR-1 is a model electroactive bacterium whose extracellular electron transfer (EET) pathway includes a sequential network of *c*-type cytochromes that span the inner membrane, periplasm, and outer membrane. While electrochemical studies have revealed the critical role of outer-membrane cytochromes in mediating both outward EET from cells to external surfaces and lateral biofilm conduction across cells, the specific functional role of periplasmic cytochromes in these processes remains less understood. Dissecting the contributions of periplasmic components has been challenged by the complexity of the periplasmic cytochrome network and the variability of native biofilms, which confound electrochemical comparisons of cytochrome mutants. Here, we overcome these limitations with a synthetic biology approach combining targeted deletion of genes encoding key periplasmic cytochromes with light-induced biofilm patterning to create uniform, geometrically defined biofilms on electrodes for robust electrochemical comparisons. Voltammetric measurements of patterned *S. oneidensis* mutant biofilms confirmed the essential role of periplasmic cytochromes in facilitating outward EET, a contribution that becomes apparent when flavins are present, accelerating interfacial electron transfer between outer-membrane cytochromes and the electrode. In contrast to this role in routing outward EET across the periplasm, electrochemical gating measurements of lateral biofilm conductivity revealed that the periplasmic cytochromes do not contribute to long-distance electron transport along cellular layers bridging electrodes. These findings provide new insights into the role of periplasmic cytochromes in *S. oneidensis*, highlighting a robust functional redundancy within the periplasmic network, and distinguish their contributions to routing outward EET across the cell envelope versus biofilm conductivity.

IMPORTANCE Microbes capable of extracellular electron transfer (EET) are central to global biogeochemical cycles and emerging bioelectrochemical technologies. In the important model EET bacterium *Shewanella oneidensis* MR-1, the outer-membrane components that interface with external surfaces are well characterized. However, the functional role of the periplasmic components linking the inner and outer membranes has remained obscured by the complex network of multiple cytochromes and biofilm heterogeneity, limiting precise comparisons across mutants. By combining light-induced biofilm patterning with electrochemical analysis, we successfully revealed the specific contributions of periplasmic cytochromes: these components are essential for facilitating outward EET across the cell envelope but do not impact lateral long-distance electron transport across the biofilm. The results refine our understanding of extracellular respiration and provide design rules for engineering living electronic materials.

Editor Jizhong Zhou, The University of Oklahoma, Norman, Oklahoma, USA

Address correspondence to James Q. Boedicker, boedicke@usc.edu, or Mohamed Y. El-Naggar, mnaggar@usc.edu.

Fengjie Zhao and Christina M. Niman contributed equally to this article. Author order was determined in order of increasing seniority.

The authors declare no conflict of interest.

See the funding table on p. 13.

Received 26 May 2026
Accepted 9 June 2026
Published 16 July 2026

KEYWORDS *Shewanella oneidensis* MR-1, periplasmic cytochromes, extracellular electron transfer, biofilms

Electroactive bacteria can use extracellular electron transfer (EET) pathways to respire on solid surfaces, such as minerals and electrodes in anoxic environments to gain energy (1, 2). *Shewanella oneidensis* and *Geobacter metallireducens* were the first electroactive bacteria discovered, and the EET pathways of these two model organisms have been well studied (1–3). The reduction of extracellular electron acceptors by *S. oneidensis* requires an outward EET pathway from the inner membrane-associated cytochrome CymA (4), across the ~23.5 nm wide periplasm (5), to the outer membrane-associated multiheme cytochrome-porin complex MtrCAB (6–8). Electrons are subsequently transferred to external electron acceptors either indirectly via soluble flavins acting as redox shuttles or directly through contact with cell surface cytochromes, flavin-cytochrome complexes, and micrometer-scale membrane extensions containing cytochromes that extend the reach of cells (9–12).

By analyzing interactions between cells and electrodes, biofilm electrochemistry provides crucial insight into the distinct modalities of electron flow in biofilms, namely outward EET and biofilm conduction. Outward EET describes the abovementioned net electron flux from cellular metabolism across the cell envelope to the electrode surface. Lateral biofilm conduction, on the other hand, refers to the long-distance electron transport process where electrons propagate across the biofilm (cell-to-cell) to bridge micrometer-scale gaps, even in the absence of metabolic turnover. In the case of outward EET, the contribution of outer-membrane components has been extensively studied with electrochemical measurements of mutants lacking outer-membrane cytochromes (10, 13). However, there has been no similar detailed electrochemical characterization of mutants deficient in periplasmic cytochromes to characterize their impact on outward EET to electrodes. In the context of biofilm conduction, recent electrochemical gating measurements of *S. oneidensis* biofilms bridging interdigitated electrodes showed the crucial role of outer-membrane cytochromes in mediating long-distance electron transport along and across cells (14, 15), but the extent to which periplasmic cytochromes participate in this micrometer-scale conduction network remains an open question (16).

Previous work based on protein structure modeling and cytochrome interactions has assumed that periplasmic cytochromes diffusively link the inner-membrane cytochrome CymA and the outer-membrane cytochrome MtrA to allow electron transport across the periplasm in *S. oneidensis* (17–19). Studies have shown that periplasmic cytochromes CctA (STC) and FccA contribute to the reduction of soluble electron acceptors (such as Fe^{3+}) (20–22). Additionally, overexpression of CctA (STC) has been shown to increase current production and power density during electrochemical measurements (21, 22). However, there has not yet been a systematic study of the contributions of *S. oneidensis* periplasmic cytochromes during electron transfer to external electrodes or during lateral biofilm conduction across electrodes. The diversity of the cytochromes present in the *S. oneidensis* periplasm has complicated efforts to fully understand their roles in EET. Recently, the complexity of the periplasmic cytochrome network in the model electroactive microorganism *Geobacter sulfurreducens* has been studied using gene deletion, metal-reduction assays, and electrochemical measurements (23). The results demonstrated a lack of specificity among different periplasmic cytochromes during electron transfer, and none were required when cells utilized electrodes (23). These findings further raise the question of the role that periplasmic cytochromes play in *S. oneidensis* EET, the answer to which will deepen our understanding of EET mechanisms.

Electroactive bacteria can colonize electrode surfaces and form living, conductive biofilms (24). Electrochemical techniques, such as cyclic voltammetry and electrochemical gating, are used to characterize conductive biofilms, as they can uncover underlying electron transport mechanisms and extract material properties (14, 25, 26). To study the role of periplasmic cytochromes in *S. oneidensis* EET, it is necessary to construct

periplasmic cytochrome–deficient *S. oneidensis* mutants and perform electrochemical measurements to compare the electrochemical activity of mutant and wild-type (WT) strains. Over the past decade, synthetic biology and genome-editing tools have been developed in *S. oneidensis* to delete cytochrome genes or to regulate gene expression to probe how certain cytochromes participate in electron transfer (27–30). However, unlike *G. sulfurreducens*, native *S. oneidensis* biofilms form patchy, non-uniform structures on electrodes (14), thereby introducing significant cross-electrode variability and confounding the subtle electrochemical phenotypic differences between cytochrome mutants. To address this issue, we recently developed a lithographic strategy to pattern *S. oneidensis* biofilms by using the light-induced genetic circuit pDawn to control the expression of cell-aggregation protein CdrAB (31). This system ensures the formation of thick, uniform biofilms with a defined geometry on electrodes (31), thereby facilitating consistent and reliable electrochemical comparisons of biofilms. In addition, this approach allowed quantification of the intrinsic lateral biofilm conductivity (31).

In this work, we combined synthetic biology and electrochemical techniques to study the role periplasmic cytochromes play in both *S. oneidensis* outward EET to electrodes and lateral biofilm conductivity. Two mutants, Δ*cctA*Δ*fccA* and Δ*cctA*Δ*fccA*Δ*nrfA*, lacking genes encoding the most prominent periplasmic cytochromes (20), were constructed and used in this study. We measured the soluble iron reduction capabilities of these mutants and the wild type. With this validation, we then used cyclic voltammetry and electrochemical gating to investigate the electrochemical activity and conductive properties of patterned biofilms of our mutants. Our results indicate that periplasmic cytochromes participate in electron transfer to electrodes (outward flow of electrons from the cell) but do not contribute to the lateral biofilm conductivity. These findings deepen our understanding of the mechanisms *S. oneidensis* implements to transport electrons across its periplasm, offering insights into developing strategies to improve the EET efficiency of living biofilms.

RESULTS

Iron reduction assays validate that periplasmic cytochromes contribute to the reduction of soluble electron acceptors

A previous study showed that the periplasmic cytochromes CctA (STC), a small tetraheme cytochrome, and FccA, a tetraheme cytochrome/fumarate reductase, are involved in the reduction of soluble electron acceptors, such as ferric iron, DMSO, and nitrate (20). We first quantified soluble iron reduction capabilities of the wild type and our periplasmic cytochrome–deficient mutants using a ferrozine assay. The results show that the double mutant Δ*cctA*Δ*fccA* exhibits a significant delay in iron reduction compared to the WT (Fig. 1). Deleting the gene *nrfA*, which encodes a periplasmic pentaheme cytochrome and nitrite reductase (32), further delays soluble iron reduction in the triple mutant Δ*cctA*Δ*fccA*Δ*nrfA*. This suggests that NrfA also contributes to the reduction of soluble iron (Fig. 1). After the lag phase, the double and triple mutants begin to reduce soluble iron and eventually produce amounts of Fe^{2+} equivalent to those of the WT (Fig. 1). The times required for the double and triple mutants to fully reduce the soluble iron are around threefold longer than that of the WT. We checked the cytochrome expression of the triple mutant Δ*cctA*Δ*fccA*Δ*nrfA* at different time points during the iron reduction assay. MtrA abundance appeared to increase after the lag phase (Fig. S1), suggesting that MtrA may function both as part of the MtrCAB conduit and independently to facilitate periplasmic electron transfer. These results are consistent with a previous study (20), which reported a long lag phase in the growth of Δ*cctA*Δ*fccA* with iron citrate as the electron acceptor, along with higher MtrA expression after the lag phase. In summary, our results indicate that the periplasmic cytochromes CctA (STC), FccA, and NrfA participate in *S. oneidensis* soluble iron reduction.

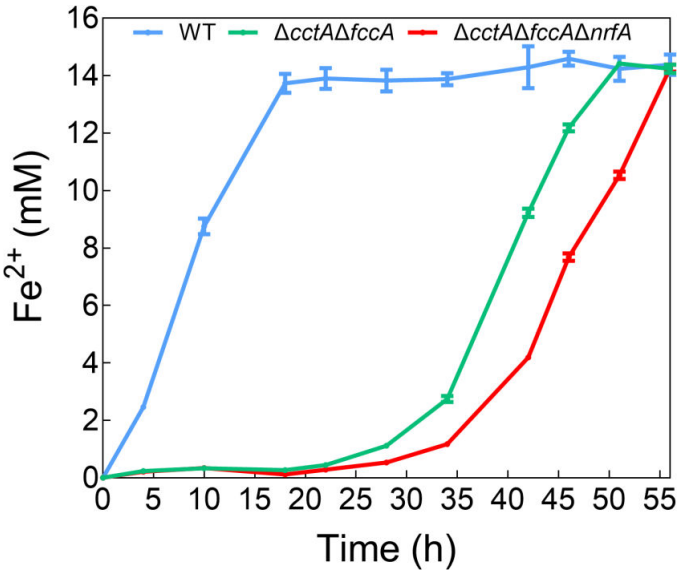

FIG 1 Measurements of iron reduction by *S. oneidensis* show that the periplasmic cytochrome–deficient mutants exhibit a significant delay compared to the wild type. WT: wild-type strain. The data (mean ± SD) were obtained from triplicate measurements.

Biofilm patterning enables uniform biofilm formation of periplasmic cytochrome–deficient mutants

Next, the contribution of periplasmic cytochromes to electron transfer between *S. oneidensis* biofilms and electrodes was analyzed. Reliably comparing biofilm EET activity across *S. oneidensis* strains and mutants is often hindered by their patchy and nonuniform coverage on electrodes. To overcome this limitation, we utilized a genetic circuit to improve *S. oneidensis* biofilm formation (31). This circuit enables light-regulated production of the cell aggregation proteins CdrAB, leading to the formation of thicker and more uniform biofilms and allowing high-resolution, light-directed patterning of *S. oneidensis* biofilms with diverse defined geometries (31). We transformed the plasmid pDawn-CdrAB, containing the biofilm patterning circuit, into the *S. oneidensis* strains used for electrochemical measurements. These new strains were named Δ*cctA*Δ*fccA* + CdrAB and Δ*cctA*Δ*fccA*Δ*nrfA* + CdrAB. The wild type transformed with the pDawn-CdrAB plasmid was named WT + CdrAB.

To verify the compatibility of the biofilm patterning construct in the context of our periplasmic deletion strains, a cell-cell aggregation assay was performed. Aggregation of cells following light-induced expression of CdrAB suggests that the strains possess improved biofilm formation capabilities (Fig. 2A). The aggregation index, which measures the reduction of the culture turbidity at the top of the culture tube after settling, shows higher values of WT + CdrAB, Δ*cctA*Δ*fccA* + CdrAB, and Δ*cctA*Δ*fccA*Δ*nrfA* + CdrAB strains than that of the WT strain (Fig. 2B). These results indicate significant cell-cell adhesion in Δ*cctA*Δ*fccA* + CdrAB and Δ*cctA*Δ*fccA*Δ*nrfA* + CdrAB strains after illumination.

To facilitate electrochemical measurements, we also demonstrated biofilm patterning of these strains on the surface of transparent electrodes. Cells were cultured in custom vessels made by vertically attaching a glass tube to a conductive, planar indium tin oxide (ITO)-coated glass coverslip (Fig. 2C). Rectangular patterns of blue light were projected onto the bottom of the ITO coverslip from below using a portable LED projector (Fig. 2C). The results show clear rectangular biofilm patterns with similar geometries for all three strains after crystal violet staining on the surface of the ITO electrodes (Fig. 2D). We also imaged the patterned biofilms via confocal microscopy, which shows dense and uniform biofilms with a thickness of ~10 µm (Fig. 2E; Fig. S2) (31). These results indicate that the patterned biofilms of the three strains are highly similar in geometry,

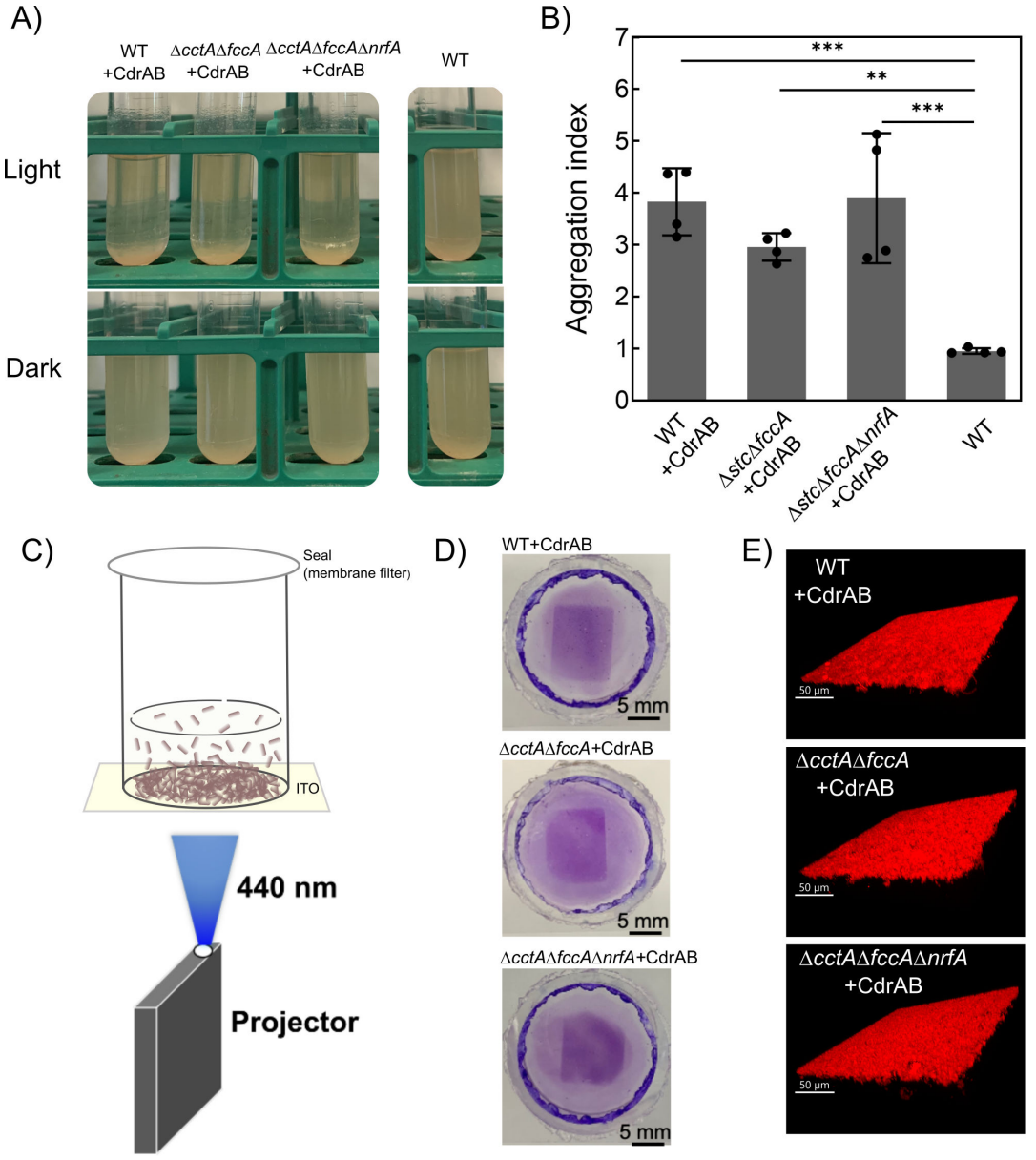

FIG 2 Cell-cell aggregation assays and biofilm patterning experiments indicate biofilm formation in different *S. oneidensis* strains can be controlled and patterned with similar geometries using light. Cell-cell aggregation assay (A) and aggregation index measurements (B) of WT, WT + CdrAB, Δ*cctA*Δ*fccA* + CdrAB, and Δ*cctA*Δ*fccA*Δ*nrfA* + CdrAB. For the aggregation index, data (mean ± SD) were obtained from four biological replicates. $P = 0.0003$ for WT + CdrAB vs. WT, $P = 0.0051$ for Δ*cctA*Δ*fccA* + CdrAB vs. WT, and $P = 0.0002$ for Δ*cctA*Δ*fccA*Δ*nrfA* + CdrAB vs. WT (one-way ANOVA with Dunnett's multiple comparisons test). Significance is indicated as ***$P < 0.001$ and **$P < 0.01$. (C) Schematic diagram of light-induced biofilm patterning on an ITO electrode in our custom glass-tube culturing vessel, using a portable LED projector. (D) Crystal violet staining of patterned biofilms with identical geometries. (E) Confocal microscope images of patterned biofilms with similar thicknesses. Images show three-dimensional confocal reconstructions generated using Imaris software. The black background corresponds to the default rendering background used by the software and is not part of the underlying confocal image data.

enabling reliable comparison of their EET activity. When our custom vessel was used ahead of electrochemical measurements, a thin copper wire was electrically connected to the ITO coverslip before cell culturing and patterning. After patterning onto the wired ITO coverslip, the reference and counter electrodes were added to the vessel, thereby enabling it to serve as a bioreactor for electrochemical measurements (Fig. 3A).

Periplasmic cytochromes participate in EET to the electrodes

Biofilm patterning enables controlled biofilm formation, enabling more reproducible electrochemical measurements compared to native biofilms (Fig. S2) (31). This allows for the direct comparison of electrochemical results among different mutants and reactors. To study whether periplasmic cytochromes contribute to electron transfer to an electrode, we performed cyclic voltammetry measurements on patterned biofilms of WT + CdrAB, Δ*cctA*Δ*fccA* + CdrAB, and Δ*cctA*Δ*fccA*Δ*nrfA* + CdrAB on the ITO glass coverslip with a defined geometry of 1.2 cm × 1.0 cm (Fig. 3A). The voltammograms revealed that the current generation of Δ*cctA*Δ*fccA* + CdrAB and Δ*cctA*Δ*fccA*Δ*nrfA* + CdrAB was nearly identical to the WT + CdrAB strain (Fig. S3A), and that all three strains have similar maximum current densities (Fig. S3B).

The similar current production by all three strains was surprising because the periplasmic cytochrome-deficient mutants show clear phenotypes for delayed iron reduction capability, but no obvious phenotype for electrode reduction. We reasoned that this could be due to electron transfer through the *S. oneidensis* periplasmic space not being a rate-limiting step under our experimental conditions, where extracellular flavins are absent. Instead, we propose that the interfacial (i.e., cell-to-electrode) electron transfer becomes rate-limiting in the absence of flavins, as previous experimental and computational studies have shown that flavins enhance this step by interacting with flavin-binding sites on the outer-membrane cytochromes or by acting as extracellular redox shuttles (9, 33–35). In our electrochemical measurements, repeated washing and replacement with fresh, flavin-free minimal medium removed extracellular flavins, making the final interfacial electron transfer step likely rate-limiting. To examine how enhancing this interfacial step may affect our investigation, we conducted additional electrochemical measurements for the patterned biofilms of WT + CdrAB and Δ*cctA*Δ*fccA*Δ*nrfA* + CdrAB, in which different concentrations of flavins were exogenously added. The representative cyclic voltammograms show that the currents produced by Δ*cctA*Δ*fccA*Δ*nrfA* + CdrAB are lower than those of the WT + CdrAB when 4.8 µM FMN is added (Fig. 3B), while the voltammograms of WT + CdrAB and Δ*cctA*Δ*fccA*Δ*nrfA* + CdrAB overlap without FMN addition (Fig. 3B). The differences in the voltammograms between WT + CdrAB and Δ*cctA*Δ*fccA*Δ*nrfA* + CdrAB become more pronounced as more FMN is added (Fig. S4). Figure 3C shows the maximum currents from the WT + CdrAB and Δ*cctA*Δ*fccA*Δ*nrfA* + CdrAB voltammograms as a function of FMN addition (Fig. 3C). The results indicate that there is no obvious difference between the maximum currents of WT + CdrAB and Δ*cctA*Δ*fccA*Δ*nrfA* + CdrAB without exogenous FMN addition (Fig. 3C). However, a lower maximum current is observed from Δ*cctA*Δ*fccA*Δ*nrfA* + CdrAB, as

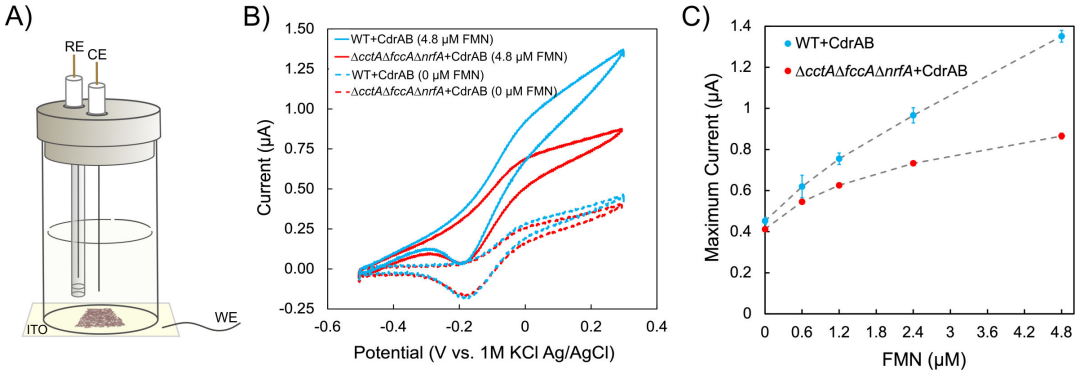

FIG 3 Electrochemical measurements of patterned WT + CdrAB and Δ*cctA*Δ*fccA*Δ*nrfA* + CdrAB biofilms on transparent ITO electrodes indicate that periplasmic cytochromes contribute to outward EET to electrodes. (A) Schematic diagram of the bioreactor with patterned biofilms for electrochemical measurements. RE: reference electrode; CE: counter electrode; WE: working electrode. (B) Representative cyclic voltammograms of light-patterned biofilms of WT + CdrAB and Δ*cctA*Δ*fccA*Δ*nrfA* + CdrAB with 0 µM and 4.8 µM flavin mononucleotide (FMN) added. (C) Effect of adding increasing concentrations of FMN on the maximum current of light patterned biofilms of WT + CdrAB and Δ*cctA*Δ*fccA*Δ*nrfA* + CdrAB. The data (mean ± SD) were obtained from two biological replicates.

compared to WT + CdrAB, with the first addition of 0.6 µM FMN. Increasing differences between the maximum currents of WT + CdrAB and Δ*cctA*Δ*fccA*Δ*nrfA* + CdrAB arise with each successive addition of FMN (Fig. 3C).

Taken together, we combined light-induced biofilm patterning and electrochemical measurements to study the electrode reduction phenotype of periplasmic cytochrome-deficient mutants. These results indicate that the periplasmic cytochromes participate in shuttling electrons through the periplasmic space during electrode reduction. This contribution is most apparent when flavins are added to eliminate interfacial cell-electrode electron transfer limitations.

Periplasmic cytochromes do not impact lateral biofilm conductivity

In addition to interfacial electron transfer to electrodes, electroactive biofilms can act as living electronic materials, allowing for long-distance electron transport across neighboring cells on the micrometer scale (36). Previous studies demonstrated a crucial role for cell surface multiheme cytochromes in this biofilm conduction (14–16), but the extent to which periplasmic cytochromes may participate in the conduction mechanism is yet to be investigated. To determine the role of periplasmic cytochromes in biofilm conductivity, we patterned WT + CdrAB and Δ*cctA*Δ*fccA*Δ*nrfA* + CdrAB biofilms with a defined geometry (1.2 cm × 1.0 cm) onto custom ITO interdigitated array (IDA) electrodes by culturing the cells in custom vessels (Fig. 2C) with a transparent ITO IDA electrode serving as the bottom. The ITO IDA electrode contains two electrically isolated conductive regions that function as source and drain electrodes with an interspersed nonconductive region (Fig. 4A). To measure the conduction current through the patterned biofilms bridging the source and drain electrodes, electrochemical gating measurements were performed after biofilm patterning. When performing electrochemical gating measurements, the potentials at each working electrode are swept across a defined range while a potential offset (V_{SD}) is maintained between the source and drain working electrodes to serve as a driving force for conduction. Figure 4B shows representative conduction current data for WT + CdrAB and Δ*cctA*Δ*fccA*Δ*nrfA* + CdrAB biofilms patterned onto IDAs with 20 µm insulating gaps. By plotting the conduction current (I_{cond}) vs the gate potential (E_G, average potential of the working electrodes during the gating scan), we observe a conduction peak centered at the formal potential of *S. oneidensis* cytochromes for both WT + CdrAB and Δ*cctA*Δ*fccA*Δ*nrfA* + CdrAB (Fig. 4B), consistent with a redox conduction mechanism (25). Both WT + CdrAB and Δ*cctA*Δ*fccA*Δ*nrfA* + CdrAB show overlapping conduction currents and statistically indistinguishable peak magnitudes (Fig. 4B; Fig. S5). With the known peak conduction current, defined biofilm geometry, and uniform biofilm thickness (~10 µm for patterned biofilms), we calculated the conductivity of the WT + CdrAB and Δ*cctA*Δ*fccA*Δ*nrfA* + CdrAB biofilms to be 6.4 ± 0.9 nS/cm and 6.0 ± 0.9 nS/cm, respectively (Fig. 4C). No significant difference in conductivity was observed between the two strains. These results indicate that the periplasmic cytochromes do not contribute to lateral biofilm conductivity.

Electron conduction through biofilms bridging electrodes stems from both heterogeneous and homogeneous electron transport processes. Heterogeneous electron transport refers to electron injection/ejection between the electrodes and the biofilm, while homogeneous electron transport refers to electron transport across and between cells within the biofilm. To further confirm that our conductivity measurements reflect conditions in which homogeneous electron transport within the biofilm is rate limiting, rather than heterogeneous EET at the biofilm-electrode interface, we performed scan rate-dependent non-turnover cyclic voltammetry of patterned WT + CdrAB biofilms on IDAs (25). Figure S6 shows the representative voltammograms collected at eight different scan rates spanning from 1 to 200 mV/s with V_{SD} = 0.0 V. Under these conditions, the resulting current is solely due to the charging and discharging of redox cofactors in the biofilm. The scaling relationship between the current and the scan rate provides information as to whether the rate-limiting step for biofilm conduction is homogeneous

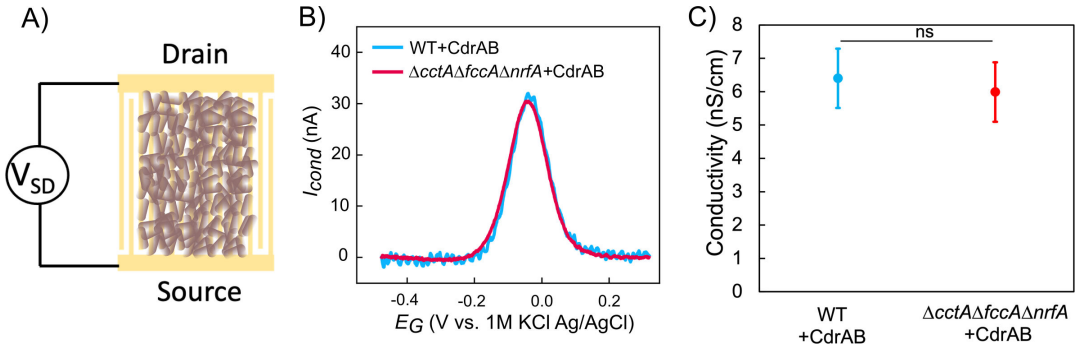

FIG 4 Electrochemical gating measurements of conductivity in WT + CdrAB and Δ*cctA*Δ*fccA*Δ*nrfA* + CdrAB patterned biofilms on ITO interdigitated array electrodes show that periplasmic cytochromes do not affect lateral biofilm conductivity. (A) Schematic diagram of the electrode configuration used in electrochemical gating measurement of patterned biofilms on IDA electrodes. (B) Representative conduction currents of patterned WT + CdrAB and Δ*cctA*Δ*fccA*Δ*nrfA* + CdrAB biofilms on IDAs. (C) Conductivities of patterned WT + CdrAB and Δ*cctA*Δ*fccA*Δ*nrfA* + CdrAB biofilms extracted from the peak conduction currents and known biofilm and electrode geometries. No significant difference in conductivity was observed between patterned WT + CdrAB biofilms and Δ*cctA*Δ*fccA*Δ*nrfA* + CdrAB biofilms (two-tailed unpaired *t*-test, $P = 0.6021$). Data are presented as mean ± SD from three biological replicates. Significance is indicated as ns (not significant, $P > 0.05$).

(i.e., between cells) or heterogeneous (i.e., between cells and the electrode) electron transfer (25). The peak currents observed in the data increase with increasing scan rate and scale linearly with the square root of the scan rate (Fig. S6, inset). The positions of the peaks do not change with increasing scan rate. These results show that the rate-limiting step in electron transport is diffusion within the biofilms, rather than electron transfer at the electrode-biofilm interface. Therefore, the similar conductivity values of WT + CdrAB and Δ*cctA*Δ*fccA*Δ*nrfA* + CdrAB biofilms measured from our electrochemical gating experiments reflect nearly identical electron transport within the biofilm.

DISCUSSION

Periplasmic cytochromes are expected to mediate electron flux between the inner and outer membranes in *S. oneidensis* (17–19), thereby facilitating outward EET to external electron acceptors. However, their role has so far been directly assessed only in reducing soluble electron acceptors. In this work, we studied the role of periplasmic cytochromes in soluble iron reduction, outward EET to electrodes, and lateral biofilm conduction across electrodes by combining synthetic biology strategies with electrochemical techniques. Outer-membrane cytochromes, such as MtrC, were previously shown to be important for soluble iron reduction (37). Since periplasmic cytochromes CctA (STC) and FccA are thought to carry electrons to the outer-membrane MtrCAB complex, we first measured the iron citrate reduction capabilities of periplasmic cytochrome–deficient mutants. Our results indicate that all periplasmic cytochromes (CctA [STC], FccA, and NrfA) play a role in iron reduction but also that *S. oneidensis* possesses a mechanism to compensate for the activity of the missing cytochromes over time. These results are consistent with a previous study, which showed that while the double mutant Δ*cctA*Δ*fccA* had a lag phase in growth with soluble iron as the electron acceptor, it could catch up to the growth of wild type by upregulating the expression levels of MtrA and NrfA (20). In our work, MtrA also appeared to have increased expression in the triple mutant Δ*cctA*Δ*fccA*Δ*nrfA* after the lag phase during soluble iron reduction (Fig. S1). These results indicate a lack of periplasmic cytochrome specificity in soluble iron reduction and that *S. oneidensis* has alternative mechanisms to recover iron reduction in the absence of CctA (STC), FccA, and NrfA. It is interesting to note that a lack of specificity for periplasmic electron transfer has also been observed recently in another model EET organism, *Geobacter sulfurreducens*, where any of six triheme cytochromes supported comparable growth on soluble or insoluble metal (23). It appears that this general promiscuity in the periplasmic electron pathways may be a general feature of outward EET.

Our initial electrochemical measurements of patterned biofilms show that deletion of the periplasmic cytochromes has no significant effect on electrode reduction without the addition of flavins (Fig. S3). However, we propose that during electrochemical measurements, the periplasmic electron transport rate was masked by the slower interfacial transfer between outer-membrane cytochromes and the electrode. Previous studies have shown that the efficiency of this interfacial step is enhanced when flavins are present to interact with flavin-binding sites on the outer-membrane cytochromes or act as soluble redox shuttles (9, 33–35). Accordingly, under our experimental conditions in which extracellular flavins were washed out prior to biofilm electrochemistry, the final electron transfer between outer-membrane cytochromes and the electrode is rate-limiting, regardless of which periplasmic cytochromes are present. With flavin addition, the electron transfer through the periplasm can become rate-limiting, making the role of periplasmic cytochromes observable. Consistent with this, electrochemical measurements of patterned biofilms with the addition of flavins show significantly lower current production in Δ*cctA*Δ*fccA*Δ*nrfA* + CdrAB compared to WT + CdrAB (Fig. 3). These results indicate that periplasmic cytochromes play a role in routing electron transfer across the periplasm to outer-membrane components, and their contribution becomes evident under conditions where the terminal cell-electrode step is no longer rate-limiting. This suggests that flavins can modulate the apparent contribution of periplasmic cytochromes by shifting the rate-limiting step in the EET pathway and may contribute to the apparent lack of specificity among these cytochromes. We thus conclude that, while periplasmic cytochromes play a role in electron transport across the periplasm during EET, this role does not appear to be specific to any individual cytochrome (Fig. 5). *S. oneidensis* possesses sufficient electron transport machinery for moving electrons across the periplasm to meet the metabolic needs of the biofilm. Most likely, the deficiencies introduced by deleting genes encoding various periplasmic cytochromes are compensated for by alternative periplasmic cytochromes (including MtrA), as recently observed in *Geobacter* (23). Meanwhile, our previous work showed that the periplasmic fumarate reductase FccA was required for Fe-mediated electron uptake (38). Combining these findings with the present study suggests that periplasmic cytochromes are also likely involved in extracellular electron uptake in *S. oneidensis*.

Finally, the electrochemical gating results shed light on the role of the periplasmic cytochromes in biofilm conduction along/across cellular layers, bridging electrodes. Our previous studies show good agreement between the measured *S. oneidensis* biofilm conductivity (~4.5 nS/cm) from the patterned biofilms (31) and the calculated *S. oneidensis* biofilm conductivity (~7 nS/cm) based on a collision-exchange model taking into account the dynamics of outer-membrane cytochromes (16). However, any possible contribution to this process from periplasmic components remained an open question. In this work, our measured conductivities show no significant difference between the WT + CdrAB biofilms (6.4 ± 0.9 nS/cm) and the Δ*cctA*Δ*fccA*Δ*nrfA* + CdrAB biofilms (6.0 ± 0.9 nS/cm). We further ruled out that slow heterogeneous EET (between the biofilm and interdigitated electrodes) may be rate limiting in biofilm conduction, thereby obfuscating rate differences in homogeneous conduction (through the biofilm) when comparing WT + CdrAB and Δ*cctA*Δ*fccA*Δ*nrfA* + CdrAB. Our scan-rate-dependent non-turnover cyclic voltammetry measurements confirm that the rate-limiting step of biofilm conduction is electron diffusion within the biofilm, and not injection/ejection at the electrode–biofilm interface. These results indicate that the periplasmic cytochromes CctA (STC), FccA, and NrfA do not play a significant role in lateral biofilm conduction of the patterned *S. oneidensis* biofilms (Fig. 5). Consistent with this conclusion, recent work by Wen et al. showed that deletion of periplasmic cytochromes had a negligible impact on the thermal activation energy (E_a) of electron transport in *Shewanella* biofilms (15). In contrast, electrochemical gating studies of *S. oneidensis* biofilms and colonies have shown that outer-membrane cytochromes play a critical role in lateral conductivity (14, 15, 39). Our findings support a model where lateral conductivity is mediated primarily

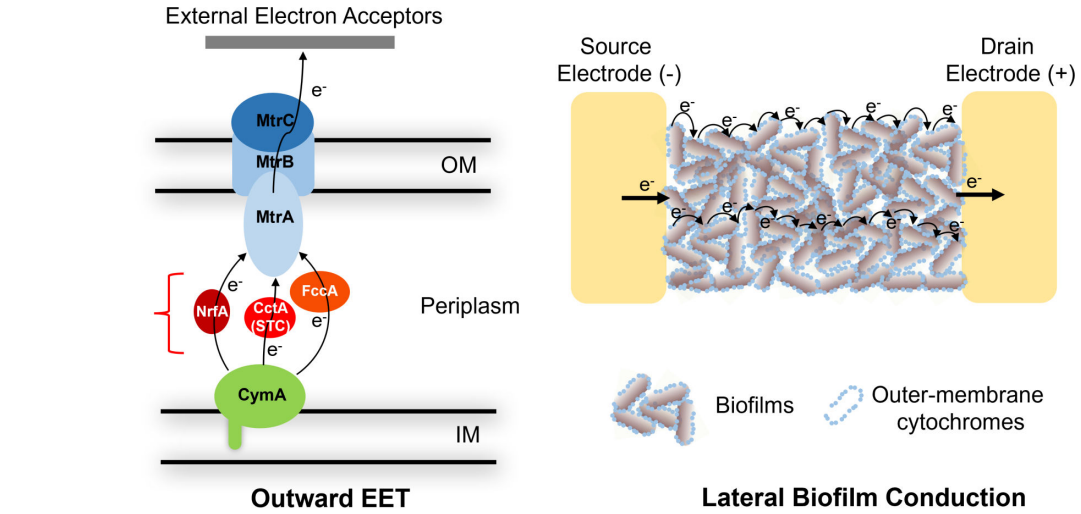

	Outward EET	Lateral Biofilm Conduction
Periplasmic cytochromes	Yes	No
Outer-membrane cytochromes	Yes (10, 13)	Yes (14-16)

FIG 5 Schematic diagram summarizing the main conclusions of this work. The left panel shows the *c*-type cytochrome network of *S. oneidensis*, including the outer-membrane MtrCAB complex, which is known to play a key role in outward EET (10, 13), as well as periplasmic cytochromes (CctA [STC], FccA, and NrfA) and the inner-membrane cytochrome CymA. Our results demonstrate that periplasmic cytochromes are involved in outward EET. The right panel shows biofilms bridging source and drain electrodes, illustrating lateral electron transport across the biofilm. Under these conditions, our results indicate that periplasmic cytochromes do not contribute to lateral biofilm conduction, while previous studies have shown that outer-membrane cytochromes are important for this process (14–16). IM, inner membrane; OM, outer membrane.

by the outer-membrane cytochrome network, consistent with the previously proposed collision-exchange mechanism (16).

The results presented in this work provide new insights into how periplasmic cytochromes participate in electron transport both across the periplasm and within biofilms (Fig. 5), which deepens our understanding of the EET mechanism in *S. oneidensis*. Our work also shows that controlling the biofilm formation of *S. oneidensis* on electrodes allows us to perform reliable comparisons of electrochemical measurements among different mutants and reactors, which is a promising strategy to quantitatively characterize EET mechanisms in other electroactive bacteria, especially those that form inconsistent biofilms.

MATERIALS AND METHODS

Bacterial strains, plasmids, and media

The strains and plasmids used in this study are listed in Table S1. The *S. oneidensis* Δ*cctA*Δ*fccA*Δ*nrfA* (JG4347) strain was generated by deleting *nrfA* in strain Δ*cctA*Δ*fccA* (JG3107) (40) utilizing materials and methods described previously (41). The blue light-induced biofilm patterning plasmid pDawn-CdrAB (31; see the plasmid map in Fig. S7 and full DNA sequence in Table S2; Addgene ID: 257836) was transformed into the Δ*cctA*Δ*fccA* and Δ*cctA*Δ*fccA*Δ*nrfA* to generate the Δ*cctA*Δ*fccA* + CdrAB and Δ*cctA*Δ*fccA*Δ*nrfA* + CdrAB strains.

S. oneidensis strains were cultivated in lysogeny broth (LB) medium (10 g/L tryptone, 5 g/L yeast extract, and 5 g/L sodium chloride) or minimal medium (15.1 g/L PIPES buffer, 3.4 g/L sodium hydroxide, 1.5 g/L ammonium chloride, 0.1 g/L potassium chloride, 0.6 g/L sodium phosphate monobasic monohydrate, 3.36 g/L 60% [wt/wt] sodium lactate,

1 mL/L mineral solution, 1 mL/L vitamin solution, 10 mL/L amino acid solution, pH 7.0) (40). For plasmid maintenance, media were supplemented with spectinomycin (Spec, 100 µg/mL). For the iron reduction assays, the minimal medium was used with 20 mM iron (III) citrate as the electron acceptor. For cyclic voltammetry measurements, the minimal medium was used without the vitamin solution to exclude the contribution from flavins. For electrochemical gating measurements, the minimal medium was used without sodium lactate and the vitamin solution. The media used for the iron reduction assays and the electrochemical measurements were purged with nitrogen.

Iron reduction assay

The ferrozine assay was used to measure Fe^{2+}—a byproduct of Fe^{3+} reduction of *S. oneidensis* strains. Cells were aerobically cultured in LB medium overnight. Cells were then collected by centrifuging (5840R, Eppendorf) at 3,234 × *g*, 4°C for 15 min and washed with fresh minimal medium two times. Cells were inoculated into sealed serum bottles containing 100 mL of anaerobic minimal medium to an OD_{600} of 0.1. An amount of 20 mM ferric citrate was added to the anaerobic minimal medium as the electron acceptor. The samples were incubated at 30°C and 200 rpm with an orbital throw of 2.5 cm. At different time points, samples were taken out from the serum bottles, and 10 µL of each sample was added immediately to 90 µL of 1 M HCl in a 96-well plate, followed by 100 µL of 0.1% ferrozine. After the samples were mixed well and allowed to sit for 10 min, the absorbance of the samples at 562 nm was determined with a plate reader (Infinite 200 PRO, Tecan). A standard curve of freshly made ferrous sulfate was used to determine the Fe^{2+} concentrations.

Cell-cell aggregation assay and biofilm patterning

The cell-cell aggregation assay was performed as described previously (31). Briefly, late log phase LB cultures of *S. oneidensis* strains were transferred into (1%, vol/vol) minimal medium and incubated aerobically overnight at 30°C and 200 rpm with an orbital throw of 2.5 cm under either blue light or dark conditions. Then, the cultures were left to rest for 30 min. The cultures in the upper regions of tubes were collected to measure the OD_{top}. Then, the cultures were rigorously vortexed for 10 s, and the OD_{total} was determined. $\frac{OD_{total}(light)/OD_{total}(dark)}{OD_{top}(light)/OP_{top}(dark)}$ was used to calculate the aggregation index.

Biofilm patterning was performed as described in our previous work (31). The late log phase LB cultures (OD_{600} about 1–1.5) were diluted into fresh minimal medium to an OD_{600} of 0.01. 1 mL of the dilution was added to the bioreactor, which was made by attaching a 20 mm diameter and 2.5 cm tall glass tube onto a transparent WE (ITO-coated glass coverslip or custom ITO IDA). The glass tube was sealed with a microporous membrane filter (AirOtop Seals) and incubated at 30°C aerobically. A portable smart projector (A5 Pro, Wowoto) was secured below the bioreactor in the incubator, and 440 nm blue light patterns created in Microsoft PowerPoint were projected onto the underside of the bioreactor (Fig. 2C). After 16 h of patterning, medium in the bioreactor was discarded, and the patterned biofilms were washed three times, for 2 min each time, with minimal medium on an orbital shaker at 60 rpm to reduce the nonspecific patterned cells. The bioreactor with fresh minimal medium was then moved to the anaerobic chamber for electrochemical measurements of the patterned biofilms. To assess biofilm formation and patterning on the electrodes, crystal violet staining was performed either immediately after patterning (if no electrochemical measurements were conducted) or after the measurements (if they were needed).

Cyclic voltammetry measurements

The cyclic voltammetry (CV) measurements were performed in an anaerobic chamber (Bactron 300, Sheldon Manufacturing, Inc.) with a 95:5 (N_2/H_2) atmosphere. After washing the patterned biofilms, the minimal medium in the bioreactor was exchanged for anoxic minimal medium without vitamin solution inside the anaerobic chamber

before CV measurements. The CV measurements were conducted with a three-electrode reactor setup. PEEK plastic lids were used with the bioreactors along with platinum wire counter electrodes (CEs) and Ag/AgCl (1 M KCl) reference electrodes (REs, CHI 111) (Fig. 3A). The PEEK plastic lids, along with CEs and REs, were not present during biofilm patterning and were only added after biofilm patterning and washing once the bioreactors were in the anaerobic chamber. The CV measurements of patterned biofilms were performed from −0.5 to 0.3 V at 1 mV/s using a four-channel potentiostat (Admiral Instruments Squidstat). Three cycles were performed for each CV, and data from only the third cycle were presented in this work. All potentials reported in this work are vs Ag/AgCl (1 M KCl).

Electrochemical gating measurements for analyzing biofilm conduction and conductivity

The custom ITO IDA electrodes were designed and fabricated as described in our previous work (31). The interdigitated area (1.2 × 1 cm^2) of the ITO IDA consisted of electrode fingers (12 mm long and 10 µm wide of each finger) and gaps (20 µm between every two fingers). The electrochemical gating measurements were performed under non-turnover conditions (minimal media without sodium lactate and vitamin solution) and conducted under a 95:5 (N_2/H_2) atmosphere in an anaerobic chamber. Like the reactor setup used for our CV measurements, platinum wire CEs and Ag/AgCl (1 M KCl) REs were inserted into the reactors through the PEEK plastic lids. Electrochemical gating measurements were performed with a potentiostat (BioLogic VSP-300). The IDA source (S) and drain (D) WEs were scanned at a rate of 1 mV/s from −0.5 to 0.3 V, but with a fixed gating offset, V_{SD} = 20 mV, where $V_{SD} = E_D - E_S$ and where E_D and E_S are the potentials at each of the IDA WEs. Three electrochemical gating cycles were performed, and data from only the third cycle were analyzed.

The conduction current I_{cond} can be extracted from the electrochemical gating measurements with the equation $I_{cond} = (I_D - I_S)/2$, where I_D is the drain current and I_S is the source current (14).

The conductivity of the patterned biofilms was calculated based on the following equations (25) as described in our previous work (31).

$$I_{cond} = G \cdot V_{SD} \quad (1)$$

$$G = \sigma \cdot S \quad (2)$$

$$S = \frac{l}{\pi} \ln\left(\frac{16g}{\pi d}\right) \quad (3)$$

Equation 1 is used to determine biofilm conductance (G). Here, I_{cond} is given by the peak conduction current and V_{SD} = 20 mV. In equation 2, G is equal to the intrinsic conductivity of the biofilm (σ) multiplied by a geometric factor (S). For the case of uniform biofilms on an IDA with a thickness on the order of the size of the finger gaps, the geometric factor S is shown as equation 3, based on a conformal mapping method. In equation 3, l is the length of the gap that snakes between the interdigitated fingers, g is the biofilm thickness, and d is the width of a finger gap.

In situ confocal microscopy observations of patterned biofilms on electrodes and biofilm thickness analysis

After electrochemical measurements, the reactor medium was discarded, and 2 mL of minimal medium containing FM 4-64FX membrane dye was added to the bioreactors to stain the biofilms for 30 min. Then, the medium was exchanged for 3% glutaraldehyde solution to fix the biofilms at 4°C overnight. Before imaging the biofilms, the samples were washed with PBS three times. A Zeiss LSM 880 inverted microscope equipped with an argon laser and a 40× water objective lens was used to image the biofilms. Imaris software was used to process confocal microscopy data and generate the 3D and cross-sectional biofilm images. Biofilm thickness measurements were performed utilizing

Matlab by analyzing the cross-sectional confocal images as described in our previous work (31).

ACKNOWLEDGMENTS

This study was supported by the US Office of Naval Research Multidisciplinary University Research Initiative Grant No. N00014-18-1-2632. The fabrication of the IDA electrodes used in this work was performed at the San Diego Nanotechnology Infrastructure (SDNI) of UCSD, a member of the National Nanotechnology Coordinated Infrastructure, which is supported by the National Science Foundation (Grant ECCS-2025752). J.T.A. was supported by the NSF Postdoctoral Research Fellowships in Biology Program under grant no. 2010604.

AUTHOR AFFILIATIONS

[1]Department of Physics and Astronomy, University of Southern California, Los Angeles, California, USA
[2]Omenn-Darling Bioengineering Institute, Princeton University, Princeton, New Jersey, USA
[3]Department of Civil and Environmental Engineering, Princeton University, Princeton, New Jersey, USA
[4]BioTechnology Institute and Department of Plant and Microbial Biology, University of Minnesota–Twin Cities, Saint Paul, Minnesota, USA
[5]Department of Biological Sciences, University of Southern California, Los Angeles, California, USA
[6]Department of Chemistry, University of Southern California, Los Angeles, California, USA

AUTHOR ORCIDs

Fengjie Zhao http://orcid.org/0000-0003-2279-5062
Christina M. Niman http://orcid.org/0009-0004-4224-6057
Marko S. Chavez http://orcid.org/0009-0005-3846-9749
Joshua T. Atkinson http://orcid.org/0000-0001-9293-4123
Bridget E. Conley http://orcid.org/0000-0002-2986-764X
Jeffrey A. Gralnick https://orcid.org/0000-0001-9250-7770
James Q. Boedicker http://orcid.org/0000-0003-4107-3719
Mohamed Y. El-Naggar http://orcid.org/0000-0001-5599-6309

FUNDING

Funder	Grant(s)	Author(s)
Office of Naval Research	N00014-18-1-2632	Fengjie Zhao Christina M. Niman Marko S. Chavez Joshua T. Atkinson Bridget E. Conley Jeffrey A. Gralnick James Q. Boedicker Mohamed Y. El-Naggar
National Science Foundation	2010604	Joshua T. Atkinson

AUTHOR CONTRIBUTIONS

Fengjie Zhao, Conceptualization, Data curation, Formal analysis, Investigation, Methodology, Software, Validation, Visualization, Writing – original draft, Writing – review

and editing | Christina M. Niman, Conceptualization, Data curation, Formal analysis, Investigation, Methodology, Software, Validation, Visualization, Writing – original draft, Writing – review and editing | Marko S. Chavez, Formal analysis, Investigation, Methodology, Writing – review and editing | Joshua T. Atkinson, Investigation, Methodology, Writing – review and editing | Bridget E. Conley, Methodology, Resources, Writing – review and editing | Jeffrey A. Gralnick, Conceptualization, Methodology, Resources, Writing – review and editing | James Q. Boedicker, Conceptualization, Funding acquisition, Investigation, Methodology, Project administration, Resources, Supervision, Writing – review and editing | Mohamed Y. El-Naggar, Conceptualization, Formal analysis, Funding acquisition, Investigation, Methodology, Project administration, Resources, Supervision, Writing – original draft, Writing – review and editing

DIRECT CONTRIBUTION

This article is a direct contribution from Mohamed Y. El-Naggar, a Fellow of the American Academy of Microbiology, who arranged for and secured reviews by Buz Barstow, Cornell University, and Ariel Furst, Massachusetts Institute of Technology.

ADDITIONAL FILES

The following material is available online.

Supplemental Material

Supplemental material (mBio01264-26-s0001.pdf). Figures S1-S7; Tables S1 and S2.

REFERENCES

1. Myers CR, Nealson KH. 1988. Bacterial manganese reduction and growth with manganese oxide as the sole electron acceptor. Science 240:1319–1321. https://doi.org/10.1126/science.240.4857.1319
2. Lovley DR, Phillips EJP. 1988. Novel mode of microbial energy metabolism: organic carbon oxidation coupled to dissimilatory reduction of iron or manganese. Appl Environ Microbiol 54:1472–1480. https://doi.org/10.1128/aem.54.6.1472-1480.1988
3. Gralnick JA, Bond DR. 2023. Electron transfer beyond the outer membrane: putting electrons to rest. Annu Rev Microbiol 77:517–539. https://doi.org/10.1146/annurev-micro-032221-023725
4. McMillan DGG, Marritt SJ, Butt JN, Jeuken LJC. 2012. Menaquinone-7 is specific cofactor in tetraheme quinol dehydrogenase CymA. J Biol Chem 287:14215–14225. https://doi.org/10.1074/jbc.M112.348813
5. Dohnalkova AC, Marshall MJ, Arey BW, Williams KH, Buck EC, Fredrickson JK. 2011. Imaging hydrated microbial extracellular polymers: comparative analysis by electron microscopy. Appl Environ Microbiol 77:1254–1262. https://doi.org/10.1128/AEM.02001-10
6. Hartshorne RS, Reardon CL, Ross D, Nuester J, Clarke TA, Gates AJ, Mills PC, Fredrickson JK, Zachara JM, Shi L, Beliaev AS, Marshall MJ, Tien M, Brantley S, Butt JN, Richardson DJ. 2009. Characterization of an electron conduit between bacteria and the extracellular environment. Proc Natl Acad Sci USA 106:22169–22174. https://doi.org/10.1073/pnas.0900086106
7. White GF, Shi Z, Shi L, Wang Z, Dohnalkova AC, Marshall MJ, Fredrickson JK, Zachara JM, Butt JN, Richardson DJ, Clarke TA. 2013. Rapid electron exchange between surface-exposed bacterial cytochromes and Fe(III) minerals. Proc Natl Acad Sci USA 110:6346–6351. https://doi.org/10.1073/pnas.1220074110
8. Edwards MJ, White GF, Butt JN, Richardson DJ, Clarke TA. 2020. The crystal structure of a biological insulated transmembrane molecular wire. Cell 181:665–673. https://doi.org/10.1016/j.cell.2020.03.032
9. Marsili E, Baron DB, Shikhare ID, Coursolle D, Gralnick JA, Bond DR. 2008. *Shewanella* secretes flavins that mediate extracellular electron transfer. Proc Natl Acad Sci USA 105:3968–3973. https://doi.org/10.1073/pnas.0710525105
10. Coursolle D, Baron DB, Bond DR, Gralnick JA. 2010. The Mtr respiratory pathway is essential for reducing flavins and electrodes in *Shewanella oneidensis*. J Bacteriol 192:467–474. https://doi.org/10.1128/JB.00925-09
11. Pirbadian S, Barchinger SE, Leung KM, Byun HS, Jangir Y, Bouhenni RA, Reed SB, Romine MF, Saffarini DA, Shi L, Gorby YA, Golbeck JH, El-Naggar MY. 2014. *Shewanella oneidensis* MR-1 nanowires are outer membrane and periplasmic extensions of the extracellular electron transport components. Proc Natl Acad Sci USA 111:12883–12888. https://doi.org/10.1073/pnas.1410551111
12. Xu S, Jangir Y, El-Naggar MY. 2016. Disentangling the roles of free and cytochrome-bound flavins in extracellular electron transport from *Shewanella oneidensis* MR-1. Electrochim Acta 198:49–55. https://doi.org/10.1016/j.electacta.2016.03.074
13. Baron D, LaBelle E, Coursolle D, Gralnick JA, Bond DR. 2009. Electrochemical measurement of electron transfer kinetics by *Shewanella oneidensis* MR-1. J Biol Chem 284:28865–28873. https://doi.org/10.1074/jbc.M109.043455
14. Xu S, Barrozo A, Tender LM, Krylov AI, El-Naggar MY. 2018. Multiheme cytochrome mediated redox conduction through *Shewanella oneidensis* MR-1 cells. J Am Chem Soc 140:10085–10089. https://doi.org/10.1021/jacs.8b05104
15. Wen X, Long X, Huang W, Kuramochi M, Okamoto A. 2025. Cell-surface inter-cytochrome electron transfer limits biofilm electron conduction kinetics in *Shewanella oneidensis*. J Am Chem Soc 147:46932–46940. https://doi.org/10.1021/jacs.5c10357
16. Chong GW, Pirbadian S, Zhao Y, Zacharoff LA, Pinaud F, El-Naggar MY. 2022. Single molecule tracking of bacterial cell surface cytochromes reveals dynamics that impact long-distance electron transport. Proc Natl Acad Sci USA 119:e2119964119. https://doi.org/10.1073/pnas.2119964119
17. Edwards MJ, White GF, Lockwood CW, Lawes MC, Martel A, Harris G, Scott DJ, Richardson DJ, Butt JN, Clarke TA. 2018. Structural modeling of an outer membrane electron conduit from a metal-reducing bacterium suggests electron transfer via periplasmic redox partners. J Biol Chem 293:8103–8112. https://doi.org/10.1074/jbc.RA118.001850
18. Fonseca BM, Paquete CM, Neto SE, Pacheco I, Soares CM, Louro RO. 2013. Mind the gap: cytochrome interactions reveal electron pathways across the periplasm of *Shewanella oneidensis* MR-1. Biochem J 449:101–108. https://doi.org/10.1042/BJ20121467
19. Alves MN, Neto SE, Alves AS, Fonseca BM, Carrêlo A, Pacheco I, Paquete CM, Soares CM, Louro RO. 2015. Characterization of the periplasmic redox network that sustains the versatile anaerobic metabolism of *Shewanella oneidensis* MR-1. Front Microbiol 6:665. https://doi.org/10.3389/fmicb.2015.00665

20. Sturm G, Richter K, Doetsch A, Heide H, Louro RO, Gescher J. 2015. A dynamic periplasmic electron transfer network enables respiratory flexibility beyond a thermodynamic regulatory regime. ISME J 9:1802–1811. https://doi.org/10.1038/ismej.2014.264
21. Delgado VP, Paquete CM, Sturm G, Gescher J. 2019. Improvement of the electron transfer rate in *Shewanella oneidensis* MR-1 using a tailored periplasmic protein composition. Bioelectrochemistry 129:18–25. https://doi.org/10.1016/j.bioelechem.2019.04.022
22. Sun W, Lin Z, Yu Q, Cheng S, Gao H. 2021. Promoting extracellular electron transfer of *Shewanella oneidensis* MR-1 by optimizing the periplasmic cytochrome *c* network. Front Microbiol 12:727709. https://doi.org/10.3389/fmicb.2021.727709
23. Choi S, Chan CH, Bond DR. 2022. Lack of specificity in *Geobacter* periplasmic electron transfer. J Bacteriol 204:e00322-22. https://doi.org/10.1128/jb.00322-22
24. Zacharoff LA, El-Naggar MY. 2017. Redox conduction in biofilms: from respiration to living electronics. Curr Opin Electrochem 4:182–189. https://doi.org/10.1016/j.coelec.2017.09.003
25. Yates MD, Golden JP, Roy J, Strycharz-Glaven SM, Tsoi S, Erickson JS, El-Naggar MY, Calabrese Barton S, Tender LM. 2015. Thermally activated long range electron transport in living biofilms. Phys Chem Chem Phys 17:32564–32570. https://doi.org/10.1039/c5cp05152e
26. Snider RM, Strycharz-Glaven SM, Tsoi SD, Erickson JS, Tender LM. 2012. Long-range electron transport in *Geobacter sulfurreducens* biofilms is redox gradient-driven. Proc Natl Acad Sci USA 109:15467–15472. https://doi.org/10.1073/pnas.1209829109
27. Corts AD, Thomason LC, Gill RT, Gralnick JA. 2019. Efficient and precise genome editing in *Shewanella* with recombineering and CRISPR/Cas9-mediated counter-selection. ACS Synth Biol 8:1877–1889. https://doi.org/10.1021/acssynbio.9b00188
28. Coursolle D, Gralnick JA. 2012. Reconstruction of extracellular respiratory pathways for iron(III) reduction in *Shewanella oneidensis* strain MR-1. Front Microbiol 3:56. https://doi.org/10.3389/fmicb.2012.00056
29. West EA, Jain A, Gralnick JA. 2017. Engineering a native inducible expression system in *Shewanella oneidensis* to control extracellular electron transfer. ACS Synth Biol 6:1627–1634. https://doi.org/10.1021/acssynbio.6b00349
30. Cao Y, Li X, Li F, Song H. 2017. CRISPRi-sRNA: transcriptional-translational regulation of extracellular electron transfer in *Shewanella oneidensis*. ACS Synth Biol 6:1679–1690. https://doi.org/10.1021/acssynbio.6b00374
31. Zhao F, Chavez MS, Naughton KL, Niman CM, Atkinson JT, Gralnick JA, El-Naggar MY, Boedicker JQ. 2022. Light-induced patterning of electroactive bacterial biofilms. ACS Synth Biol 11:2327–2338. https://doi.org/10.1021/acssynbio.2c00024
32. Gao H, Yang ZK, Barua S, Reed SB, Romine MF, Nealson KH, Fredrickson JK, Tiedje JM, Zhou J. 2009. Reduction of nitrate in *Shewanella oneidensis* depends on atypical NAP and NRF systems with NapB as a preferred electron transport protein from CymA to NapA. ISME J 3:966–976. https://doi.org/10.1038/ismej.2009.40
33. Hong G, Pachter R. 2016. Bound flavin-cytochrome model of extracellular electron transfer in *Shewanella oneidensis*: analysis by free energy molecular dynamics simulations. J Phys Chem B 120:5617–5624. https://doi.org/10.1021/acs.jpcb.6b03851
34. Okamoto A, Hashimoto K, Nealson KH, Nakamura R. 2013. Rate enhancement of bacterial extracellular electron transport involves bound flavin semiquinones. Proc Natl Acad Sci USA 110:7856–7861. https://doi.org/10.1073/pnas.1220823110
35. Breuer M, Rosso KM, Blumberger J. 2015. Flavin binding to the deca-heme cytochrome MtrC: insights from computational molecular simulation. Biophys J 109:2614–2624. https://doi.org/10.1016/j.bpj.2015.10.038
36. Atkinson JT, Chavez MS, Niman CM, El-Naggar MY. 2023. Living electronics: a catalogue of engineered living electronic components. Microb Biotechnol 16:507–533. https://doi.org/10.1111/1751-7915.14171
37. Coursolle D, Gralnick JA. 2010. Modularity of the Mtr respiratory pathway of *Shewanella oneidensis* strain MR-1. Mol Microbiol 77:995–1008. https://doi.org/10.1111/j.1365-2958.2010.07266.x
38. Abuyen K, El-Naggar MY. 2023. Soluble iron enhances extracellular electron uptake by *Shewanella oneidensis* MR-1. ChemElectroChem 10:e202200965. https://doi.org/10.1002/celc.202200965
39. Tokunou Y, Tongu H, Kogure Y, Okamoto A, Toyofuku M, Nomura N. 2024. Colony-based electrochemistry reveals electron conduction mechanisms mediated by cytochromes and flavins in *Shewanella oneidensis*. Environ Sci Technol 58:4670–4679. https://doi.org/10.1021/acs.est.4c00007
40. Zhao F, Niman CM, Ostovar G, Chavez MS, Atkinson JT, Bonis BM, Gralnick JA, El-Naggar MY, Boedicker JQ. 2024. Red-light-induced genetic system for control of extracellular electron transfer. ACS Synth Biol 13:1467–1476. https://doi.org/10.1021/acssynbio.3c00684
41. Ross DE, Flynn JM, Baron DB, Gralnick JA, Bond DR. 2011. Towards electrosynthesis in *Shewanella*: energetics of reversing the Mtr pathway for reductive metabolism. PLoS One 6:e16649. https://doi.org/10.1371/journal.pone.0016649